The effects of grooves on wind characteristics of tall cylinder buildings

Wei-bin Yuan[1,2], Nan-ting Yu[*3] and Zhao Wang[1]

[1]*College of Architecture and Civil Engineering, Zhejiang University of Technology, Hangzhou, 310014, PR China*
[2]*Key Laboratory of Civil Engineering Structures & Disaster Prevention and Mitigation*
Technology of Zhejiang Province, Hangzhou, 310014, PR China
[3]*School of Engineering, University of Plymouth, Plymouth, PL4 8AA, United Kingdom*

Abstract. For most full-scale tall buildings the Reynolds number of a flow field around a circular cylinder under strong wind is usually greater than 2×10^7, which is difficult to achieve in most wind tunnel tests. To explore the wind characteristics of tall cylindrical buildings with equidirectional grooves from subcritical to transcritical flow ($6.6\times10^4 \leq Re \leq 3.3\times10^5$ and $9.9\times10^6 \leq Re \leq 7.2\times10^7$), wind tunnel tests and full-scale large eddy simulations were carried out. The results showed that the rectangular-grooves narrow the wake width due to the downstream movement of the separation point and the deeper grooves cause smaller mean and fluctuating pressure while the peak pressure is little affected. Furthermore, the grooves lead to lower frequency of vortex shedding but the Strouhal number remains at the range from 0.15 to 0.35. The drag coefficient of the cylinders with grooves was found to be 2~3 times as large as that of smooth cylinders.

Keywords: tall cylinder buildings; wind characteristics; wind tunnel test; large eddy simulation

1. Introduction

For nearly half a century, many high rise buildings have been constructed, most of which have complicated facades and involve vertical balconies. As a result, the wind characteristics of such buildings may be influenced globally and/or locally by the use of facades. Particular attention was paid to wind load around a tall circular building owing to its unique characteristics, which has been investigated intensely, largely by using the methods of experiments and/or numerical simulations.

Generally, the surface roughness, whose heights are lower than the boundary layer around the body, not only contributes to the boundary-layer transition from laminar to turbulent, but also affects significantly the subsequent flow development at Reynolds number beyond its critical value. It was showed that a small roughness coefficient could be influential on the flow past a seemingly smooth circular cylinder at high Reynolds number (Nakamura and Tomonari 1982). Existing studies have focused on the effects of roughness and groove sizes and ranges of Reynolds number on the flow characteristics around the cylinder using experimental methods. Table 1 lists some arrangements of roughness sizes and Reynolds number published in literature for rough or smooth cylinders.

The examination of these data shows that, most roughness coefficients used are limited in a small order of magnitude (i.e., less than 10-2) while the Reynolds numbers are in comparatively larger ranges (i.e., at least 103 and up to 107). These data, however, do not cover many modern tall buildings having large groove sizes. It is known that the large size grooves can have profound effect on the wake flow around the structure, the turbulence statistics and the frequency of vortex shedding. Canpolat (2015) examined the features of the flow passing a circular cylinder with a single longitudinal groove pattern placed on its surface. His results show that the presence of the grooves on a cylinder surface significantly affected the wake flow pattern and the turbulence statistics. Recently, Canpolat and Sahin (2017) investigated the flow control mechanism of single longitudinal groove on a circular cylinder surface with different angles.

Previous experiments have been devoted to the analysis of flow around a cylinder. Maruta *et al.* (1998) carried out an experimental study to examine the reduction of wind pressures on glass and claddings of buildings with rectangular cross section with various roughness types. Tsutomu Adachi (1997) used cylinders with various equidirectional surface roughness and sizes of grooves to investigate the Strouhal number in the wake flow of a cylinder over a wide range of Reynolds numbers. Achenbach and Heinecke (1981) did a similar work but focused on the vortex shedding from smooth and rough cylinders. Zhou *et al.* (2015) examined the force and flow characteristics of circular cylinders with different types of artificial surface roughness. They reported that certain configuration of surface roughness reduces the mean drag coefficient and the root-mean-square lift coefficient is considerably low when compared to that of a similar smooth cylinder. Recently, experimental measurements of wind pressure on the surface roughness of cylinders were also reported, for example, by Belloli *et al.* (2014), Wong and Lam (2013), Zuo (2014).

Apart from the experimental studies described above, computational fluid dynamics (CFD) has been extensively used as an efficient tool for the prediction of fluid

*Corresponding author, Ph.D.
E-mail: nanting.yu@plymouth.ac.uk

Table 1 Arrangements of roughness and Reynolds number published in literature

Published Cases	t/D	Re
Hinsberg and Paul (2015)	1.2×10^{-3}	$1.5 \times 10^{4} \sim 1.2 \times 10^{6}$
Tsutomu Adachi (1997)	$4.54 \times 10^{-6} \sim 2.5 \times 10^{-3}$	$5.0 \times 10^{4} \sim 1.0 \times 10^{7}$
Achenbach and Heinecke (1981)	$7.5 \times 10^{-4} \sim 3.0 \times 10^{-2}$	$6.0 \times 10^{3} \sim 5.0 \times 10^{6}$
Yamagishi and Oki (2005)	1.04×10^{-2}	$1.0 \times 10^{4} \sim 1.0 \times 10^{5}$
Kiu *et al.* (2011)	$2.8 \times 10^{-3} \sim 1.38 \times 10^{-2}$	$1.7 \times 10^{4} \sim 8.3 \times 10^{4}$
Nakamura and Tomonari (1982)	$6.5 \times 10^{-5} \sim 1.0 \times 10^{-2}$	$4.0 \times 10^{4} \sim 1.7 \times 10^{6}$

characteristics in wind engineering (Blocken 2014, Gousseau *et al.* 2013, Hanjalić and Kenjereš 2008, Mo et *al.* 2013, Tamura 2008). Among available turbulence models, theory of Large Eddy Simulation (LES), supported by ever increasing computing resources, is well developed and suitable for simulating the three-dimensional flow of large-scale structures with anisotropic turbulent scalar fluxes. LES is superior to both Reynolds Average Navier-Stokes (RANS) and the Unsteady Reynolds Average Navier-Stokes (URANS) in terms of physical modeling intrinsically (Blocken 2015). The comparisons of various turbulence models have been reported in literature (Lubcke 2001, Kim *et al.* 2015b, Murakami 1993a, b, Parnaudeau *et al.* 2008, Rodi 1997). In addition, LES has been employed in investigating the flow field around a cylinder and predicting the wind pressure (Fröhlich and Rodi 2004, Hu *et al.* 2015, Franke 2002, Köse and Dick 2010, Kim *et al.* 2015a, Lu *et al.* 2012, Ouvrard *et al.* 2010). Moreover, Prsic *et al.* (2014) investigated the three-dimensional flow around a circular cylinder in a steady and uniform current at subcritical Reynolds number. Catalano *et al.* (2003) assessed the viability and accuracy of LES for a circular cylinder at high Reynolds number, which demonstrated that the LES is more accurate than the RANS. Existing work in both experiments and numerical simulations focused on the high buildings with smooth surface, while in many modern buildings the form of external elevation is diverse and grooves are more commonly used, especially in the form of balcony. In addition, the Reynolds number of most full-scale tall buildings under the condition of strong winds can reach to supercritical region (Re>2×10⁷) for which case most wind tunnel test apparatus almost cannot meet. Hence, for large number of real-world applications, a better understanding of the effect of rectangular-groove on wind characteristics at high Reynolds number under various surface conditions is required. In the present study, both the wind tunnel tests and full-scale LES are employed to investigate the effects of equidirectional grooves with large roughness coefficients (t/D=0.25~0.1) on the wind characteristics of tall cylinder buildings. Firstly, the models with smooth and different groove sizes were tested in the wind tunnel (6.6×10⁴≤Re≤3.3×10⁵). Then a full-scale computational domain and corresponding tall cylindrical building models were built to simulate the interaction between wind and buildings. Finally, the distribution of wind pressure coefficient, including mean, fluctuating and peak pressures, and the mean drag coefficients and Strouhal number dependency on Reynolds number were examined and are discussed based on different groove sizes.

2. Experimental details

2.1 Wind tunnel tests

The experiments were performed at wind tunnel laboratory of Zhejiang University, China. The dimensions of the working section of the wind tunnel are 3 m high, 4 m wide and 18 m long. The range of available wind speeds is 3~55 m/s. Based on the cylinder diameter and the wind speed used (set as 10~50 m/s, measured by 4 channel hot-wire anemometer system), the Reynolds number, estimated by using the cylinder size and the actual wind speed, was in the range from 6.6 ×10⁴ to 3.3 ×10⁵, covering both subcritical and supercritical flows around an isolated cylinder (Schewe 1983). Triangular spires and 5 m long fetches of floor roughness elements were employed to develop the turbulent boundary layer flows (see Fig. 1). Fig. 2(a) shows the experimental and theoretical profiles of mean wind speed and turbulence intensity. Also, it should be mentioned here that the corresponding turbulence intensity was Iz=10% approximately at the buildings height, and the mean wind speed profile followed well the power law with an exponent of α=0.16. The measured spectrum of along-wind turbulence was well agreed compared to the target Von Karman spectrum, as shown in Fig. 2(b).

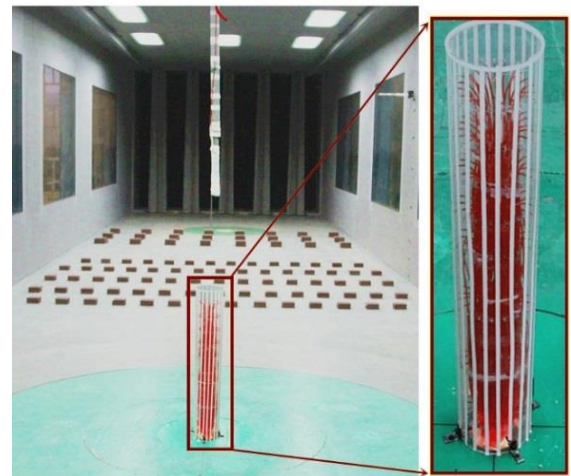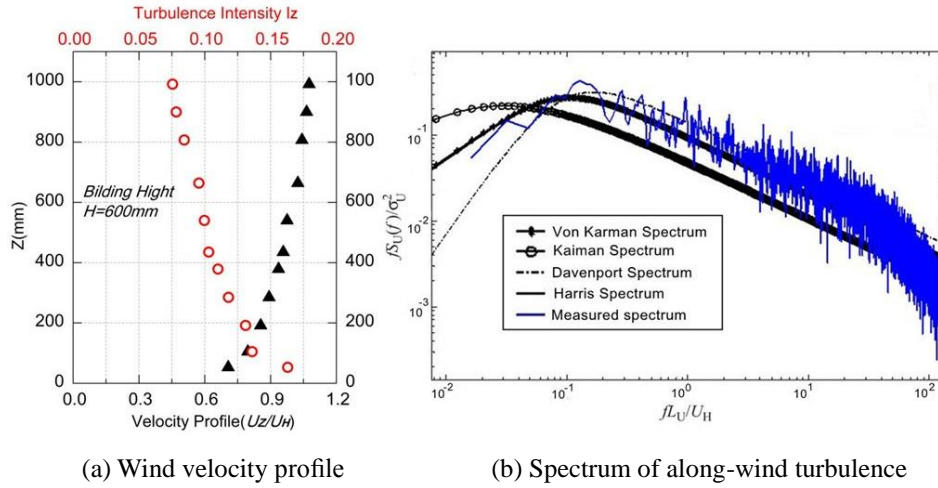Fig. 1 Wind tunnel and the model

(a) Wind velocity profile   (b) Spectrum of along-wind turbulence

Fig. 2 Wind characteristics imposed at model location

Table 2 Groove size of models used in experiments

Models	Groove coefficient(t/D)	Size in full scale (m)
M0	0	0
M1	1/40	0.75
M2	1/20	1.50
M3	3/40	2.25
M4	1/10	3.00

2.2 Models and the measurement

For the purpose of obtaining high structural quasi-static behavior and frequencies under wind flow, much attention was paid to make the model as rigid as possible. Table 2 shows the arrangement of roughness coefficient in the wind tunnel tests and full scale sizes, respectively. All the models were made of organic glass with geometric scale of 1:300, which gives rise to the fact that the blockage ratio is 0.5%.

The basic model has the height of H=600 mm and the circular cross-section with the diameter of D=100 mm, corresponding to 180 m and 30 m in full scale, respectively. Simultaneously, the protruding surface rough elements were made up of long-striped plastic with different groove coefficient t/D (where t is the thickness of the grooves and D is cylinder diameter, shown in Fig. 3) and installed on the surface of the smooth models along the vertical direction, where t/D=0 means smooth surface.

In regard to the measurement, measuring points were embedded in the center of each concave. There are 20 measuring points on each level (i.e., one measuring point every 18 degrees). Each model has eight levels (marked with A~H), giving a total of 160 measurement points. Wind pressures of each tap were measured at a sampling frequency of 312.5 Hz and recorded simultaneously by a Pitot-static tube (outer diameter of 1.6 mm) via a multi-channel pressure transducer connected to scanivalve and processed on a microcomputer. The total number of measured data was about 10,000 with a recording length of 32 s for each measuring point, corresponding to 40 min

in full scale based on the time scale of 1/75 and velocity scale of 1/4. Due to the effects of measuring tubes, numerical compensations were employed to modify the distortions of fluctuating wind pressures by using the transfer function method (Xie and Gu 2005). Fig. 3 graphically shows the cross section of cylinder and distribution of measuring points and grooves at the section.

3. Numerical simulations

3.1 Large eddy simulation

For the purpose of obtaining the wind characteristics of the cylinder comprehensively, the three-dimensional LES was carried out based on the FLUENT module of ANSYS. In order to get rid of high frequency fluctuations, the approach of LES employed consists of filtering Navier–Stokes equations, in which the effect of small eddies was calculated using a sub-grid scale model. In FLUENT, a filtering operation is executed by implicit finite-volume discretization and the large-scale mean value is computed by
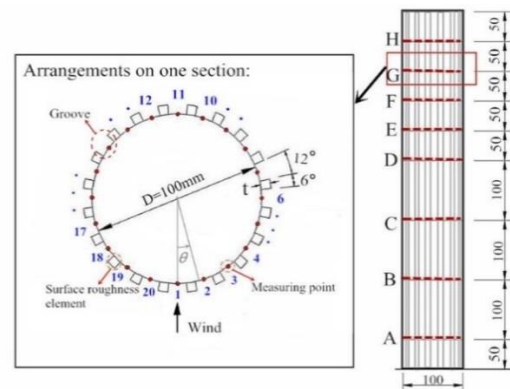

Fig. 3 Arrangement of measuring points and grooves on models

$$\bar{\phi} = \int_D \phi G(x, x') \, dx' \tag{1}$$

where ϕ is the unfiltered function, D is the flow region, x' is the spatial coordinate, x is the filtered spatial coordinate, and G(x, x') is the filter function, which defines the large and small eddies. In other words, it retains the variability of ϕ among the scales greater than the width. G(x, x') is defined as follows

$$G(x, x') = \begin{cases} \dfrac{1}{V}, x' \in V \\ 0, x' \notin V \end{cases} \tag{2}$$

where V is the volume of a computational cell. The filtered Navier–Stokes equations for a constant density fluid are expressed as follows

$$\begin{cases} \dfrac{\partial \bar{u}_i}{\partial x_i} = 0 \\ \dfrac{\partial}{\partial t}(\rho \bar{u}_i) + \dfrac{\partial}{\partial x_j}(\rho \bar{u}_i \bar{u}_j) = \dfrac{\partial \bar{\sigma}_{ij}}{\partial x_j} - \dfrac{\partial \bar{p}}{\partial x_i} - \dfrac{\partial \tau_{ij}}{\partial x_j} \end{cases} \tag{3}$$

where i, j=1, 2 and 3; u_1, u_2 and u_3 are the velocity components along x, y and z axis of the Cartesian coordinate system; σ_{ij} is the stress tensor of filtered molecular viscosity; and τ_{ij} is the stress tensor of sub-grid scale resulting from the filtering process

$$\tau_{ij} = \rho \overline{u_i u_j} - \rho \bar{u}_i \bar{u}_j \tag{4}$$

The use of filter process with variable filter width is required due to the LES of inhomogeneous turbulent flows. Ghosal and Moin (1995) neglected the spatial commutation errors that generate supplementary terms in the equations above for varying filter width spatially. In other words, Eq. (3) is correct only for a constant filter width.

Among all the sub-grid models, sub-grid stress tensor is defined as Eq. (5), which is widely used in large eddy simulation.

$$\tau_{ij} = \frac{1}{3}\tau_{kk}\delta_{ij} - 2v_t \overline{S_{ij}} \tag{5}$$

Where, $\overline{S_{ij}}$ is the rate-of-strain tensor and v_t is the sub-grid eddy viscosity. The isotropic part of the stresses is added to the pressure term because it has not been modeled. In the standard Smagorinsky-Lilly Model, the eddy viscosity is obtained from

$$v_t = \rho L_s^2 |\bar{S}| \tag{6}$$

where $|\bar{S}| = \sqrt{2\overline{S_{ij}S_{ij}}}$ and $L_S = \min(\kappa d, C_S \Delta)$ are the filtered strain rate and the mixing length for sub-grid scales, respectively, κ is the Karman constant, d is the distance to the closest wall, $C_S = [(3C_k/2)^{3/4}]/\pi$ is the Smagorinsky coefficient, and Δ is the filter width, calculated by $\Delta = V^{1/3}$, where C_k is the Kolmogorov constant and V is the volume of the computational cell. According to Lam *et al.* (2010), small values of Cs lead to converged results. In other words, large Cs values result in excessive damping of the large scale fluctuations in shear or transitional flows. Normally,

Eq. (7) can be used to adjust the Cs

$$C_S = C_{S_0}(1 - e^{y^+/A^+}) \tag{7}$$

where y^+ is the closest distance to the wall, $A^+ = 25.0$ is the semi-empirical constant and $Cs_0 = 0.1$ is called Van Driest constant. On the basis of experience-based evaluation, the use of $Cs = 0.1$ provided the most accurate results (Gousseau *et al.* 2013, Hu *et al.* 2015) and thus is also used in the present study.

For solving the unsteady uncompressible Navier–Stokes equation, the finite volume method was adopted with the algorithm of pressure implicit with splitting of operators. Moreover, the second order implicit scheme was selected to discretize time and a bounded central difference was employed for the discretization of convective terms included in the momentum equations. Apart from the choice of the calculating method, the time step is another significant parameter to choose in order to achieve accurate results. In the summary of Franke *et al.* (2011), the time step in the study was obtained from

$$\Delta t = \frac{CFL}{u_{max}} \Delta x_{min} \tag{8}$$

where, CFL is the Courant-Friedrichs-Lewy number, Δx_{min} is the minimum grid width (Δx_{min}=0.1 m) and u_{max} is the maximum along-wind velocity (u_{max}=40 m/s). Hence, in present simulations the time interval of 0.002 s was also used by considering CFL<1 for most parts of the computational domain, which is smaller than the estimate value of 0.0025 s.

3.2 Computational domain and the mesh

With reference to the full-scale height (H=180 m) and diameter (D=30 m) of the cylinder building, a full-scale 3D computational domain was modeled with the size 55D×20D×3H (x,y,z). The centre of the cylinder (and the origin of the coordinate system) is placed 15D from the inlet boundary, 2H away from the top boundaries and 40D away from the outlet boundary (Franke *et al.* 2011), as is shown in Fig. 4. A Reynolds number, ranging from 9.9 ×10⁶ to 7.2 ×10⁷, was facilitated by the full-scale dimensions of building and the along-wind velocity. Currently, the blockage ratio was only 1.7%, which is smaller than the maximum blockage of 3% proposed by Blocken (2015).

As to the numerical simulations, the results rely heavily on the quality of computational mesh in addition to the time step and solving method mentioned above. Compared with the experimental results, it was shown that the interior refined grids increase the accuracy of the numerical results (Hu *et al.* 2015). The present study adopted a hybrid grid scheme, in which the grid near the surface of building was refined enough to capture details of the flow characteristics while it was coarse in the far field comparatively. Throughout the whole computational domain, the building was nested in an interior square prism, where the grids were refined by unstructured grid whereas structured grids distribute outside the prism.
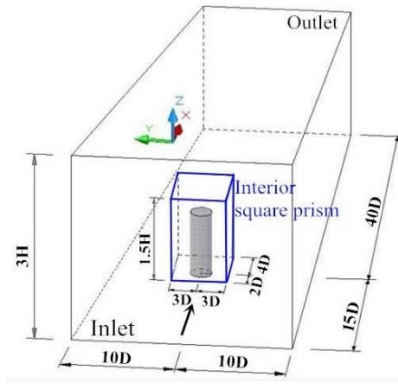
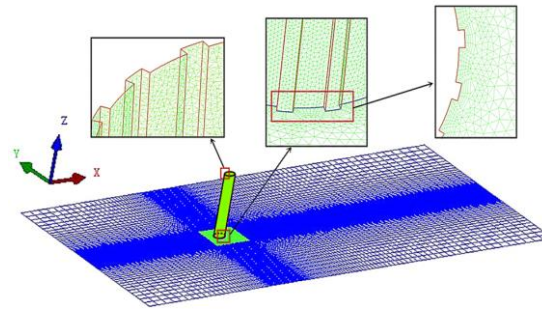Fig. 4 Dimension of the computational domain and interior refined grid domain

Fig.5 Details of mesh arrangement

Table 3 Configuration and the testing result of interior refined grid

Grid types	Total grid cells	$Re(\times 10^7)$	Layer of prism grid	St	Cd
G1	4,357,183	7.2	2	0.138	1.939
G2	8,125,306	7.2	4	0.152	1.744
G3	13,479,290	7.2	6	0.167	1.615

Fig.5 shows the details of the mesh arrangement. What is worth mentioning is that the tested building was surrounded by a viscous boundary layer with a 6-layers prism grid and the height of the first layer was small enough to satisfy the requirement of the wall unit distribution.

Three substantially interior refined grids, marked with G1, G2 and G3, were tested prior to taking the present numerical grids, considering the impact of the grid quality on the simulative results. The configuration of the grids and part of the testing results are listed in Table 3.

The mean drag coefficient (*Cd*) and the Strouhal number (*St*) were employed to evaluate the testing results preliminary, which are defined as

$$\text{Cd} = \frac{F_d}{0.5\rho U_{ref}^2 D} \tag{9}$$

$$\text{St} = \frac{nD}{U_{mean}} \tag{10}$$

where, F_d is the aerodynamic force acting on the building in along-wind direction, n is the frequency of vortex shedding,

U_{mean} is the mean velocity of the incoming flow and U_{ref} is the reference velocity at the reference height, a point over the top of the cylinder.

3.3 The simulation assumptions and boundary conditions

In order to simplify the problem, the study made the assumption that the air fluid is isotropic and incompressible and, at the same time, the fluid is Newtonian fluid, ignoring the viscous dissipation. Note that the Reynolds number is dependent on the fluid speed and the characteristic length of the structure. In present study, the characteristic length of the cylinder is relatively large, whereas the fluid velocity is comparatively small (<50 m/s). Thus, the incompressible assumption for air fluid in the supercritical condition is reasonable.

The numerical simulation was performed using the SIMPLEC algorithm. The boundary conditions used were as that. (1) Inlet speed was imported using the UDF file and the inflow wind speed adopted 10 m height of annual average speed, that is 3 m/s, in Hangzhou area. The wind profile function conforms to the exponential law under

class-B ground roughness where coefficient is 0.15. (2) Outlet pressure was assumed to be 0. In addition, symmetrical boundaries were used and non-slip wall condition was assumed. The transient simulation was employed and the simulations were considered to be convergent when the residual error is less than 10^{-6} (Franke *et al.* 2011), implying that the flow field turns into a stead state.

4. Results and discussion

4.1 Validation of the simulation

Pressures, acquired from the tests and *LES*, are presented as non-dimensional pressure coefficient (*Cp*), defined as

$$Cp = \frac{p - p_0}{\rho U_{ref}^2 / 2} \qquad (11)$$

where, *p* is the time-averaged pressure and p_0 is the reference pressure, measured at a point in the upstream of the tested model, as is shown in Fig. 1. Fig. 6 presents the comparisons of mean pressure coefficients (*Cp,mean*) between numerical and experimental results, at four different angles corresponding to the windward $(0°)$,the right side $(90°)$, leeward $(180°)$ and the left side$(270°)$ for *Re*=3.3×10^5. Although there are some discrepancies in quantification, it can be seen from the figure that the results of *LES* are agree well with experimental results, particularly in the variation tendency of *Cp,mean*. Furthermore, a stagnation point occurs at a height of 70% approximately of a vertical and isolated cylinder (Holmes 2007) where the approaching flow splits into three directions (i.e. upwash, downwash and horizontal flow). Hence, *Cp,mean* values at three different levels, corresponding to the base (level-A), height of stagnation point (level-E), and near the free end (level-H) of the vertical cylinder, are compared, which are shown in Fig. 7. In spite of some acceptable discrepancies, the *Cp,mean* tendency of numerical results is well in agreement with the experimental ones for all of three levels.

In addition, the discrepancies of mean drag coefficients (*Cd,mean*) for all the cylinders between the experimental and *LES* results are weeny, and the largest difference is only around 2.5%.Table 4 lists the *Cd,mean* of the cylinders acquired in *LES* and experiments. Again, the data indicates that the *LES* results are reliable.

Table 4 Mean drag coefficients acquired from *LES* and experiments

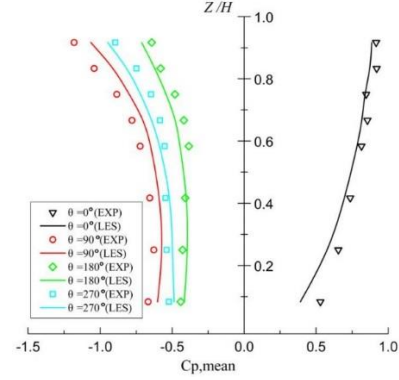| Models	$Cd,mean$ (*LES*)	$Cd,mean$ (*EXP*)	Difference (%)
M0	0.741	0.718	3.11
M1	1.317	1.290	2.08
M2	1.359	1.323	2.67
M3	1.370	1.333	2.73
M4	1.415	1.387	1.98

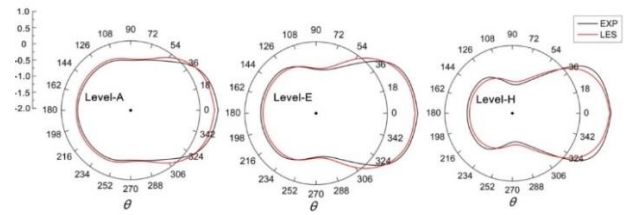Fig. 6 Comparison of mean pressure coefficients between experiments and LES at four different angles

Fig. 7 Comparisons of mean pressure coefficients between experiments and LES at three different levels

4.2 Wind pressure coefficient

4.2.1 Mean wind pressure coefficient

Both the experiments and numerical simulations were employed to investigate the pressure on the surface of the circular cylinder since the pressure is one of the most important parameters required in the design of the structure (Köse and Dick 2010, Maruta *et al.* 1998, Zuo 2014). Fig. 8 depicts the distribution of the experimentally obtained mean pressure coefficients of the smooth and rough cylinders. Because of the symmetry in geometry and the periodicity of the vertex shedding, herein only half of the measuring points (i.e., Point 1 to 11, corresponding to $\theta = 0°{\sim}180°$) are showed. It can be seen from the figure that, for the smooth cylinder the distribution of *Cp,mean* was quite similar to that reported in other studies (Catalano *et al.* 2003, Ouvrard *et al.* 2010), in which the maximum value of *Cp,mean* occurs at the front of section kernel, corresponding to θ=75° approximately (i.e., Point 5 in the present study). However, for the rough cylinder the distribution curves of *Cp,mean* slightly shaft inward and the maximum value of *Cp,mean* occurs at around θ=90°. It is seen from Fig. 8 that the largest *Cp*,mean is corresponding to t/D=1/40. The reason for happening this is because the groove elements can disturb the laminar flow structure and generate small rotating vortices in the concaves. In literature it was reported that the groove contributes to expanding the range of high velocity, or in other words, the groove elements narrow the wake width due to downstream movement of the separation point (Zdravkovich 1997). This kind of features is also demonstrated in the present simulations, which is shown in Fig. 9.
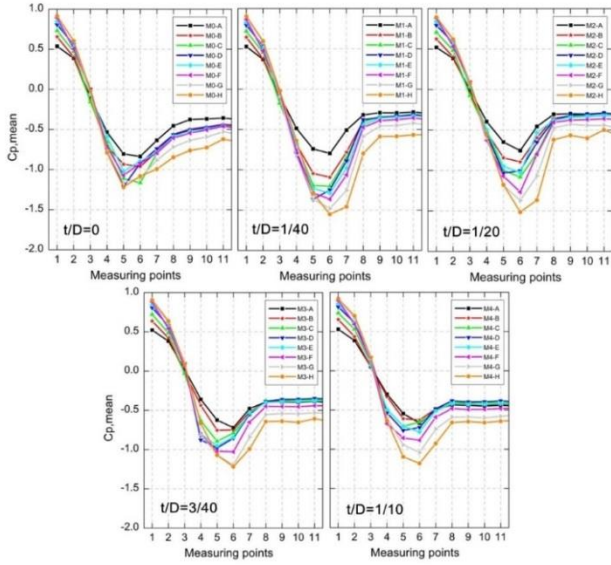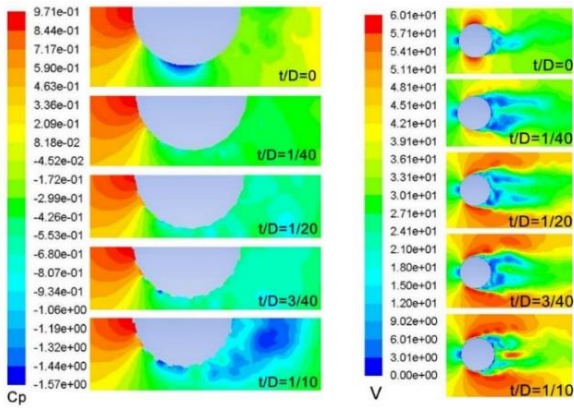
Fig. 8 Mean pressure coefficients of the smooth and rough cylinders (EXP)

(a) Pressure coefficients (b) Velocity magnitude

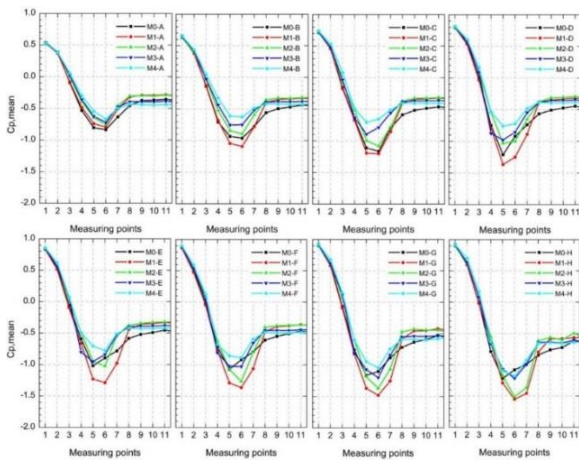Fig. 9 Contours of pressure coefficients and velocity magnitude

Also, it is noticed from Fig. 8 that there is some increase of $Cp,mean$ with the range of height from level-A to level-H. This is because the use of the mean wind velocity profile as shown in Fig. 2. However, for the same level, the value of $Cp,mean$ is highly dependent on the size of groove. Fig. 10 shows the variation of $Cp,mean$ at different levels with the grooves size, which were obtained from our experiments. It seems that, the largest absolute value of $Cp,mean$ at each level (except for at point A, near the bottom) occurs when t/D=1/40.

4.2.2 Peak and fluctuating wind pressure coefficient

Apart from the mean pressure coefficients, another important parameter is the peak value of the pressure. Fig. 11 shows the variation of both the positive and negative peak values of the mean pressure coefficient with the groove size. It can be seen that the negative peak value reaches to the maximum for M2 (i.e., t/D=1/20), whereas the positive peak value reduces to the minimum.

Fluctuating pressure, as a random action on the surface of the cylinder, is also influenced by the groove elements. As is demonstrated in Fig. 12, there is an obvious tendency that the deeper the groove is, the smaller the fluctuating pressure is. Furthermore, the high fluctuating pressure was found to associate with the increasing height in addition to level-H interfered by the three-dimensional flow over the roof.
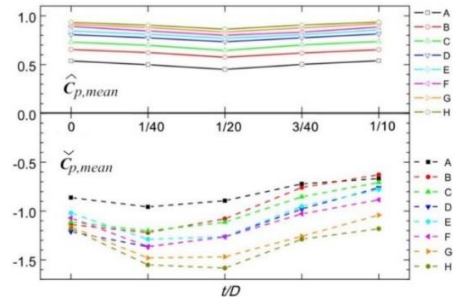

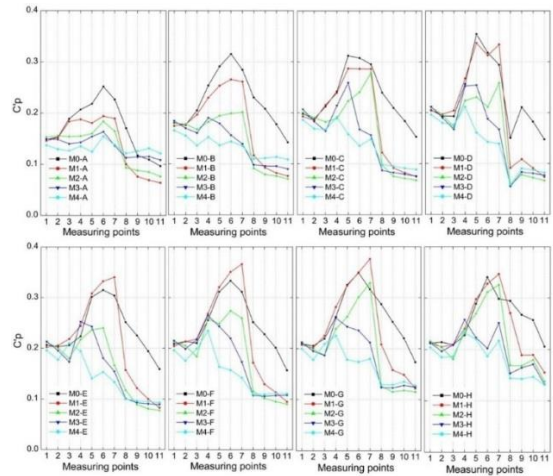Fig. 11 Positive and negative peak values of the mean pressure coefficient

Fig. 10 Mean pressure coefficients on each level (EXP)

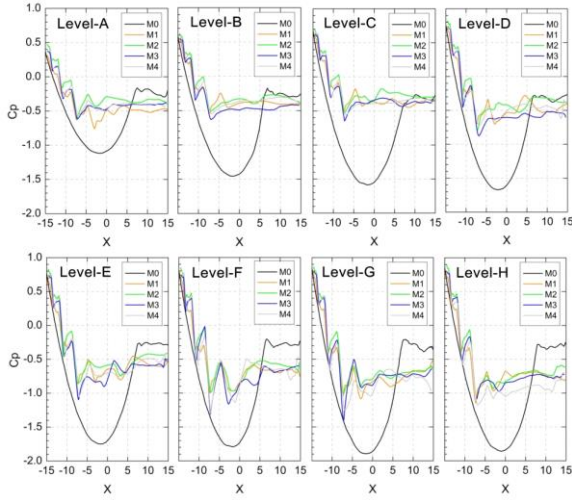Fig. 12 Fluctuating pressure coefficients (EXP)

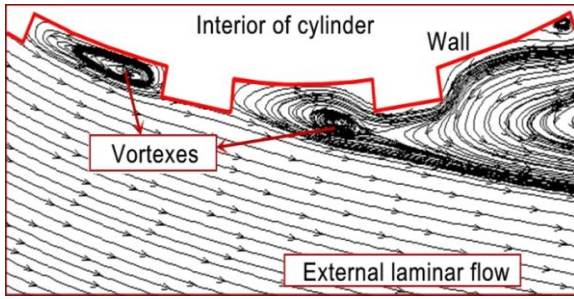Fig. 13 Pressure coefficients on each level (LES)

Fig. 14 Details of vortexes in grooves

Note that the fluctuating pressures in the rough cylinders with various groove sizes are different from that of the smooth cylinder, especially for the height of more than half (i.e., from level-E to level-H). As is shown in Fig. 12, with the height increased, the maximum value of the fluctuating pressure coefficients ($C'p$) changes from the front to the lateral, and until the posterior of section kernel, this is from point 5, 6 to point 7 in Fig. 3. Shedding, reattached of vortex and other rotating vortices exist in the internal and external of concaves, primarily contributing to the variation mentioned above besides the irregular separation of laminar flow.
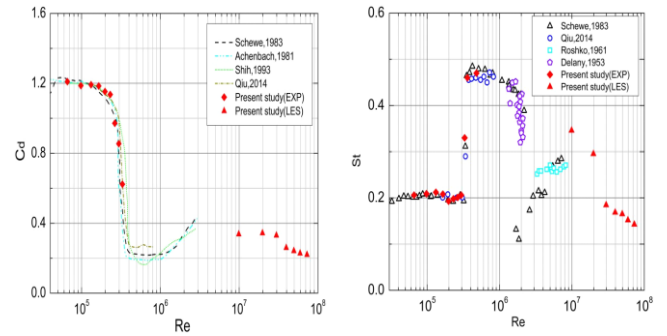
Fig. 13 shows the distribution of Cp (= $Cp,mean$ + $C'p$) obtained from *LES*. It is worth noting that Cp in rough cylinders dropped dramatically when compared to the smooth cylinder due to the effects of the convex elements, and its decreasing level in each concave relies on the size of groove elements, which lead to vortexes in the back of convex, as is shown in Fig. 14.

4.3 The mean drag coefficients and Strouhal number dependency on Reynolds number

Figs. 15 and 16 show the comparisons of the mean drag coefficient and Strouhal number obtained from the present study with those published in literature for smooth cylinder (Achenbach and Heinecke 1981, Delany 1953, Qiu *et al.*

2014, Schewe 1983, Shih *et al.* 1993). Good agreement can be seen for $6.6 \times 10^4 \le$ Re $\le 3.3 \times 10^5$. Among the range of Reynolds number from 9.9×10^6 to 7.2×10^7, however, the value of *Cd* has a trend of decrease.
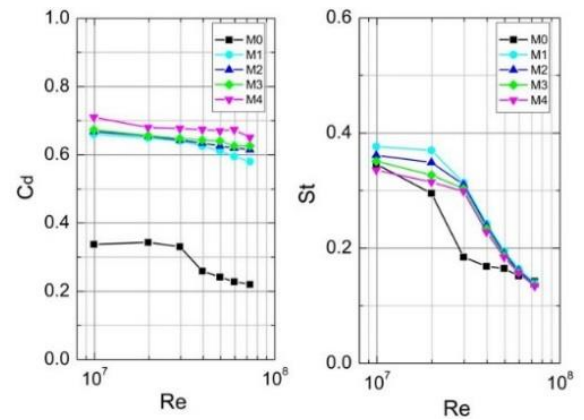
Given the fact that the air flow in nature is often turbulent, which has led to the reemergence of strong, coherent shedding than that for smooth flow (Zan 2008), many researchers published comprehensive studies on the relationship between *St* and *Re*. In turbulent flow of experiments, the value of *St* is determined by the dominant peak in the spectra of the lift fluctuations generally, corresponding to the vortices regularly shedding from the cylinder approximately. Due to the full-scale size and velocity according to actual situation, the tested Reynolds number in turbulent flow of *LES* was limited in $9.9 \times 10^6 \sim 7.2 \times 10^7$, and the data indicated that the *St* remains at the range from 0.15 to 0.35 because of the large structure rigidity of model. For rough cylinder models, *St* decreased as *t/D* and *Re* increased, as is shown in Fig.16. Furthermore, the *Cd* of the rough cylinders is 2~3 times as large as that of the smooth cylinder.

(a) Mean drag coefficients   (b) Strouhal number

Fig. 15 Comparisons of mean drag coefficient and Strouhal number with published data

(a) Mean drag coefficients   (b) Strouhal number

Fig. 16 The effect of *Re* and *t/D* on the mean drag coefficients and Strouhal number

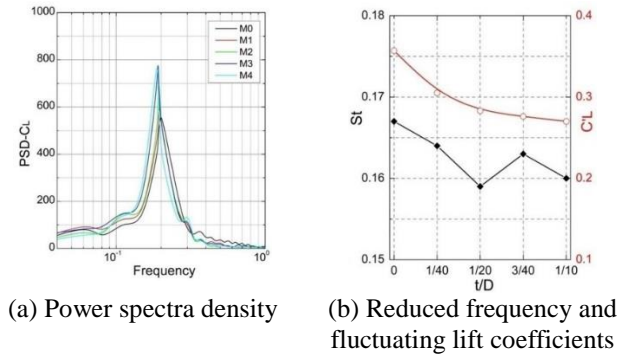| (a) Power spectra density	(b) Reduced frequency and fluctuating lift coefficients

Fig. 17 The power spectra density, reduced frequency and fluctuating lift coefficients for various groove sizes

4.4 Strouhal number based on various groove sizes at $Re=7.2\times10^7$

For most full-scale tall buildings, the Reynolds number is normally greater than 2×10^7 under strong wind. Specifically, most existing studies analyzed the smooth and rough cylinders at $Re=7.2\times10^7$ according to the time history of the instantaneous across-wind lift coefficients (C_L). On the one hand, the value of C_L for each model oscillates around 0, indicating $C_L\approx0$ and good flow symmetry about the cylinder axis; on the other hand, however, there is a significant tendency that the fluctuating lift coefficients decreased with increasing t/D, as depicted in Fig. 15(b).

Moreover, due to the periodic vortex shedding from the two sides of the cylinder, the fluctuating lift is dominated by fluctuating pressures. Therefore, the present study employed the Fast Fourier Transforms method to analyze the power spectral characteristics of C_L time history. Fig. 17(a) shows the power spectra density (*PSD*) of lift coefficients for different groove sizes at $Re=7.2\times10^7$.

It is observed from Fig. 17 that there is a distinct and definite peak around the frequency of 0.20 and the frequency spectrum width of across-wind C_L narrow down due to the vortex shedding, reattached and rotating vortices. Zhou *et al.* (2015) reported that the surface roughness plays a role in affecting frequency in the transcritical regime. Canpolat (2015) also detected relatively lower and higher frequencies of Karman vortex shedding and additional frequencies because of the grooved side of the cylinder. According to the present study, the peak value of PSD-C_L increases with the increase of t/D, whereas the frequency of periodic vortex shedding decreases with the increased t/D, as is shown in Fig. 17(b).

5. Conclusions

From the study with the use of both the experiments and numerical simulations with the condition of open surface, on five circular cylinders embedded with rectangular-grooves of different sizes, the following conclusions can be drawn:

- The presence of rectangular grooves on the circular cylinder can expand the range of high velocity and narrow the wake width due to the downstream movement of the separation point. The deeper the grooves are, the smaller the mean and fluctuating pressures are.
- The peak pressure is little affected by deeper grooves. The negative peak pressure value reaches to the maximum, whereas the positive peak pressure value reduces to the minimum when $t/D=1/20$. The boundary layer around the cylinder is disturbed when the groove height is between $t/D=1/40$ and $t/D=1/20$.
- The mean drag coefficient and Strouhal number obtained from the present study agree well with published results for $6.6\times10^4\leq Re\leq3.3\times10^5$. However, for Reynolds number ranging from 9.9×10^6 to 7.2×10^7, *St* remains at the range from 0.15 to 0.35, while the value of *Cd* of the rough cylinders is 2~3 times as large as that of the smooth cylinder.
- Groove size plays a role in affecting the frequency in the supercritical regime. The frequency of vortex shedding in full-scale simulations has the value of 0.20 at $Re=7.2\times10^7$ and the frequency spectrum width of across-wind lift coefficient narrows down due to the vortex shedding, reattached and rotating vortices.

Acknowledgments

References

Abrahamsen Prsic, M., Ong, M.C., Pettersen, B., Myrhaug, D. (2014), "Large eddy simulations of flow around a smooth circular cylinder in a uniform current in the subcritical flow regime", *Ocean Eng.*, **77**, 61-73.

Achenbach, H. (1981), "On vortex shedding from smooth and rough cylinders in the range of Reynolds number 6×10^3 to 5×10^6", *J. Fluid. Mech.*, **109**, 239-251.

Adachi, T. (1997), "Effects of surface roughness on the universal Strouhal number over the wide Reynolds number range", *J. Wind Eng. Ind. Aerod.*, **69-71**, 399-412.

Belloli, M., Rosa, L. and Zasso, A. (2014), "Wind loads and vortex shedding analysis on the effects of the porosity on a high slender tower", *J. Wind Eng. Ind. Aerod.*, **126**, 75-86.

Blocken, B. (2014), "50 years of Computational Wind Engineering: Past, present and future", *J. Wind Eng. Ind. Aerod.*, **129**, 69-102.

Blocken, B. (2015), "Computational fluid dynamics for urban physics: Importance, scales, possibilities, limitations and ten tips and tricks towards accurate and reliable simulations", *Build. Environ.*, **91**, 219-245.

Canpolat, C. (2015), "Characteristics of flow past a circular cylinder with a rectangular groove", *Flow Meas. Instrum.*, **45**, 233-245.

Canpolat, C. and Sahin, B. (2017), "Influence of single rectangular groove on the flow past a circular cylinder", *Int. J. Heat Fluid Fl.*, **64**, 79-88.

Catalano, P., Wang, M., Iaccarino, G. and Moin, P. (2003). "Numerical simulation of the flow around a circular cylinder at high Reynolds number", *Int. J. Heat Fluid Fl.*, **24**, 463-469.

Delany, N.K. and Sorensen, N.E. (1953), "Low-speed drag of

cylinders of various shapes", National Advisory Committee for
Aeronautics, 3038.

Fröhlich, J. and Rodi, W. (2004), "LES of the flow around a
circular cylinder of finite height", *Int. J. Heat Fluid Fl.*, **25**,
537-548.

Franke, J., Hellsten, A., Schlunzen, K.H. and Carissimo, B. (2011),
"The COST 732 Best Practice Guideline for CFD simulation of
flows in the urban environment: a summary", *Int J. Environ.
Pollut.*, **44**(1-4), 419-427.

Ghosal, S. and Moin, P. (1995), "The basic equations for the large-
eddy simulation of turbulent flows in complex-geometry ", *J.
Comput.Phys.*, **118**, 24-37.

Gousseau, P., Blocken, B. and van Heijst, G.J.F. (2013), "Quality
assessment of Large-Eddy Simulation of wind flow around a
high-rise building: Validation and solution verification",
Comput. Fluids, **79**, 120-133.

Lubcke, H., Rung, T. and Thiele, F. (2001), "Comparison of LES
and RANS in bluff-body flow", *J. Wind Eng. Ind. Aerod.*, **89**,
1471-1485.

Hanjalić, K. and Kenjereš, S. (2008), "Some developments in
turbulence modeling for wind and environmental engineering",
J. Wind Eng. Ind. Aerod., **96**, 1537-1570.

Hinsberg, V. and Paul, N. (2015), "The Reynolds number
dependency of the steady and unsteady loading on a slightly
rough circular cylinder: From subcritical up to high transcritical
flow state", *J. Fluid. Struct.*, **55**, 526-539.

Holmes, J.D. (2007), *Wind loading of structures*, (3th Ed.).

Hu, H.X., Liu, C.B., Hu, H.Z. and Zheng, Y.G. (2013), "Three-
dimensional numerical simulation of the flow around two
cylinders at supercritical Reynolds", *Fluid Dyn. Res.*, **45**, 1-22.

Hu, G., Tse, K.T., Kwok, K.C.S. and Zhang, Y. (2015), "Large
eddy simulation of flow around an inclined finite square
cylinder", *J. Wind Eng. Ind. Aerod.*, **146**, 172-184.

Franke, J. and Frank, W. (2002), "Large eddy simulation of the
flow past a circular cylinder at Re=3900", *J. Wind Eng. Ind.
Aerod.*, **90**, 1191-1206.

Köse, D.A. and Dick, E. (2010), "Prediction of the pressure
distribution on a cubical building with implicit LES", *J. Wind
Eng. Ind. Aerod.*, **98**, 628-649.

Kim, S., Wilson, P.A. and Chen, Z.M. (2015a), "Large-eddy
simulation of the turbulent near wake behind a circular cylinder:
Reynolds number effect", *Appl. Ocean Res.*, **49**, 1-8.

Kim, S., Wilson, P.A. and Chen, Z.M. (2015b), "Effect of
turbulence modelling on 3D LES of transitional flow behind a
circular cylinder", *Ocean Eng.*, **100**, 19-25.

Kiu, K.Y., Stappenbelt, B. and Thiagarajan, K.P. (2011), "Effects
of uniform surface roughness on vortex-induced vibration of
towed vertical cylinders", *J. Sound. Vib.*, **330**, 4753-4763.

Lam, K., Lin, Y.F., Zou, L. and Liu, Y. (2010), "Investigation of
turbulent flow past a yawed wavy cylinder", *J. Fluid. Struct.*,
26(7-8), 1078-1097.

Lu, C.L., Li, Q.S., Huang, S.H., Chen, F.B. and Fu, X.Y. (2012),
"Large eddy simulation of wind effects on a long-span complex
roof structure", *J. Wind Eng. Ind. Aerod.*, **100**, 1-18.

Maruta, E., Kanda, M. and Sato, J. (1998), "Effects on surface
roughness for wind pressure on glass and cladding of buildings",
J. Wind Eng. Ind. Aerod., **74-76**, 651-663.

Mo, J.O., Choudhry, A., Arjomandi, M. and Lee, Y.H. (2013),
"Large eddy simulation of the wind turbine wake characteristics
in the numerical wind tunnel model", *J. Wind Eng. Ind. Aerod.*,
112, 11-24.

Murakami, S. (1993a), "Comparison of various turbulence models
applied to a bluff body", *J. Wind Eng. Ind. Aerod.*, **46**, 21-36.

Murakami, S. (1993b), "Discussions of turbulence modelling and
their applications: Comparison of various turbulence models
applied to a bluff body", *J. Wind Eng. Ind. Aerod.*, **46-47**, 183-
191.

Nakamura, Y. and Tomonari, Y. (1982), "The effects of surface
roughness on the flow past circular cylinders at high Reynolds
number", *J. Fluid Mech.*, **123**, 363-378.

Ouvrard, H., Koobus, B., Dervieux, A. and Salvetti, M.V. (2010),
"Classical and variational multiscale LES of the flow around a
circular cylinder on unstructured grids", *Comput. Fluids*, **39**(7),
1083-1094.

Parnaudeau, P., Carlier, J., Heitz, D. and Lamballais, E. (2008),
"Experimental and numerical studies of the flow over a circular
cylinder at Reynolds number 3900", Phys. Fluids, 20.

Qiu, Y., Sun, Y., Wu, Y. and Tamura, Y. (2014), "Analyzing the
fluctuating pressures acting on a circular cylinder using
stochastic decomposition", *J. Fluid. Struct.*, **50**, 512-527.

Rodi, W. (1997), "Comparison of LES and RANS calculations of
the flow around bluff bodies", *J. Wind Eng. Ind. Aerod.*, **69**, 55-
57.

Rodriguez, I., Lehmkuhl, O., Piomelli, U., Chiva, J., Borrell, R.
and Oliva, A. (2017), "LES-based study of the roughness
effects on the wake of a circular cylinder from subcritical to
transcritical reynolds numbers", *Flow Turbul. Combust.*, **99**(3-
4), 729-763.

Schewe, G. (1983), "On the force fluctuations acting on a circular
cylinder in crossflow from subcritical up to transcritical
Reynolds number", *J. Fluid Mech.*, **133**, 265-285.

Shih, W.C.L., Wang, C., Coles, D. and Roshko, A. (1993),
"Experiments on flow past rough circular-cylinders at large
Reynolds-numbers", *J. Wind Eng. Ind. Aerod.*, **49**, 351-368.

Tamura, T. (2008), "Towards practical use of LES in wind
engineering", *J. Wind Eng. Ind. Aerod.*, **96**, 1451-1471.

Wong, S.Y. and Lam, K.M. (2013), "Effect of recessed cavities on
wind-induced loading and dynamic responses of a tall building",
J. Wind Eng. Ind. Aerod., **114**, 72-82.

Xie, Z.N. and Gu, M. (2005), "A correlation-based analysis on
wind-induced interference effects between two tall buildings",
Wind Struct., **8**(3), 163-178.

Yamagishi, Oki (2005), "Effect of the number of grooves on flow
characteristics around a circular cylinder with triangular
grooves", *J. Visualization*, **8**(1), 57-64.

Zan, S.J. (2008), "Experiments on circular cylinders in crossflow
at Reynolds number up to 7 million", *J. Wind Eng. Ind. Aerod.*,
96, 880-886.

Zdravkovich, M.M. (1997), "Flow around circular cylinders" vol.
1. Fundamentals, *J. Fluid Mech.*, **350**, 375-378.

Zhou, B., Wang, X., Gho, W.M. and Tan, S.K. (2015), "Force and
flow characteristics of a circular cylinder with uniform surface
roughness at subcritical Reynolds number", *Appl. Ocean Res.*,
49, 20-26.

Zuo, D.L. (2014), "Full-scale measurement of wind pressure on
the surface of an oscillating circular cylinders", *J. Wind Eng.
Ind. Aerod.*, **133**, 65-79.

CC